Available online at www.sciencedirect.com
ScienceDirect
Journal of Membrane Science 293 (2007) 1–14
journal of MEMBRANE SCIENCE
www.elsevier.com/locate/memsci

A generalized integral method for solving the design equations of dissolution/diffusion-controlled drug release from planar, cylindrical and spherical matrix devices

María I. Cabrera [1], Ricardo J.A. Grau [*,2]

Laboratorio de Química Fina, INTEC (UNL-CONICET),[3] Parque Tecnológico del Litoral Centro, Ruta Nacional 168, Paraje El Pozo, 3000 Santa Fe, Argentina

Received 4 November 2006; received in revised form 16 January 2007; accepted 18 January 2007
Available online 21 January 2007

Abstract

A versatile approach for solving the design equations of dissolution/diffusion-controlled drug release from planar, cylindrical and spherical matrix systems is provided, as an extension of a previously validated approach for planar geometry. The original set of differential mass balance equations is cast into an equivalent system of integral equations by generating appropriate Green's functions. Mathematical features common to the matrix geometry, drug diffusion process, and boundary layer resistance are imbedded in Green's functions, and thus separated from specific aspects arising from the drug dissolution process. This avoids repetitive computational effort when analyzing different drug dissolution rates. The solution for the perfect sink condition is given as a special case. Another singular feature is related to the friendly manipulation of a broad variety of spatially non-uniform drug loading, including size distribution of solid drug particles. Composite matrices consisting of multi-layers of equal diffusivity, including membranes, can be numerically simulated solving a concise dissolution–diffusion integral equation, coupled to the integral equations governing the variable surface area of the dissolving drug particles. This is made within a unique framework and without introducing extra difficulties or adjustments in the programming from one matrix architecture to another. The reliability of the approach presented is ascertained by comparing the results with existing analytical and numerical solutions for special cases, and also by matching, as asymptotic case, the numerical solution of the diffusion equation with a continuum dissolution source described by the Noyes–Whitney equation. An iterative routine, combined with the topological concept of homotopy, is used to improve the numerical performance. The versatility of the method to treat different architectures resembling multi-layer matrices of planar, cylindrical and spherical shapes is shown.

Keywords: Drug release; Dissolution/diffusion-controlled release; Matrix system; Non-uniform drug loading; Variable surface area; Simple geometries

1. Introduction

A variety of mathematical and numerical approaches have been proposed to provide some theoretical background for designing drug release matrix systems [1]. Major efforts have focused on the mathematical modeling of dispersed-drug release systems. Since its development in the early 1960s, Higuchi's model has been widely used to describe purely diffusion-controlled release of dispersed drug [2]. Further contributions, including exact and approximate solutions [3–6], non-planar geometry [7–14], non-uniform drug loading [15–18], boundary layer resistances and finite external media [5,8,17,19–23], and composite structures [17,24,25], have extended the scope of Higuchi's pioneering model. These and other contributions have furthered the mathematical description of dispersed-drug systems with fast dissolution rates, but their scope is unsuitable for examining the case of a slowly dissolving drug since the instantaneous dissolution of drugs is a common assumption. By the mid-to-late 1970s, the implications of drug dissolution as a rate-limiting step began to be studied in order to approach constant release rates. However, because of the complexity of solving the governing mass balance equations, few

* Corresponding author. Tel.: +54 342 4511539.
E-mail address: cqfina@ceride.gov.ar (R.J.A. Grau).
[1] Member of CONICET's Research Staff.
[2] Professor at UNL and member of CONICET's Research Staff.
[3] Instituto de Desarrollo Tecnológico para la Industria Química. Universidad Nacional del Litoral (UNL) and Consejo Nacional de Investigaciones Científicas y Técnicas (CONICET).

0376-7388/$ – see front matter © 2007 Elsevier B.V. All rights reserved.
doi:10.1016/j.memsci.2007.01.013

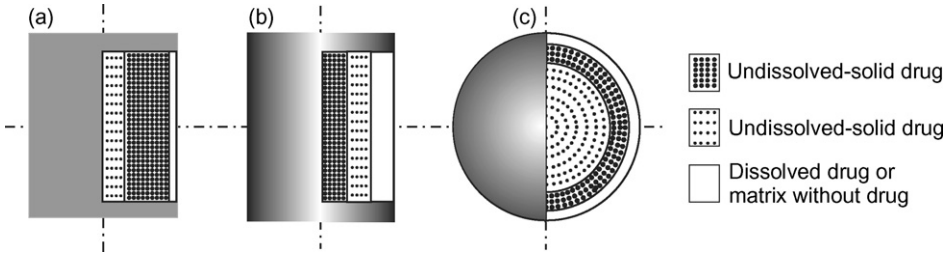

Fig. 1. Schematic illustration of one-dimensional matrix systems of (a) planar, (b) cylindrical, and (c) spherical geometry to be described within a unique mathematical framework. Dissimilar dotted regions denote layers with different solid drug loading.

contributions have been reported for this relevant case [26–32]. The most accurate descriptions include a source term in the diffusion equation to account for the drug dissolution process, and also allow for variable surface areas of the dissolving drug particles [30–32]. The dissolution source term has been usually described using a modified Noyes–Whitney type equation [33]. The models vary in their complexity, details, and solution methodology. Useful analytical short time approximations have been derived to describe the fraction of released drug [31,32]. However, the diffusion and Noyes–Whitney equations must be numerically solved in a coupled form if an accurate description of the full release process is desired.

Recently, a new approach for modeling the drug release from planar matrix systems containing slowly dissolving drugs has been proposed [34]. A distinctive feature is related to the friendly numerical manipulation of a broad variety of non-uniform drug loading and particle size distributions. Different architectures of two-layer and three-layer laminate polymeric systems, including empty layers resembling membranes, were easily solved within a unique framework, irrespective of the release system architecture. The reliability of the mathematical and numerical procedures was ascertained by comparison of the simulation results with the experimental and numerical data existing in the literature, and also matching, as asymptotic case, the solution of the diffusion equation with a continuum dissolution source described by the Noyes–Whitney equation. Nevertheless, the usefulness of this approach has still not been examined for the theoretical analysis of other simple shapes, such as the cylindrical and spherical ones.

This contribution deals with the generalization of the above-referenced approach to planar, cylindrical and spherical matrices. As the main result of this extended approach, a concise and general form of the dissolution–diffusion integral equation is obtained for all three geometries. The numerical solution uses iterative solving routines combined with the topological concept of homotopy in order to improve the numerical performance in comparison with that attainable using the standard iterative method. The versatility of the method to analyze dissolution-controlled release from single-layer and multi-layer matrix devices is demonstrated for the three geometrical shapes. A comparative study of the drug release patterns is made for different matrix architectures.

2. Mathematical model

To illustrate the points to be put forward by this contribution, matrix systems as those schematically shown in Fig. 1 will be analyzed within a unique framework, irrespective of the composed architecture. In the following analysis, all simplifying assumptions are identical to those used for the planar geometry [34]. Likewise, the dispersed-drug release device is envisaged as a primary matrix containing solid drug particles assembled on N cross-sectional areas symmetrically and arbitrarily located at $\xi_1, \xi_2, \ldots, \xi_N$ (see Fig. 2). By virtue of the continuum framework, these symmetrical assemblies are inventoried in the governing mass balance equation as drug dissolution sources. After a certain time, the exhaustion of particles begins and progresses from the outer boundary inwards the matrix, source by source, until they vanish. Release systems with drug dissolution sources evenly dispersed in the whole matrix are feasible to be approached as asymptotic case as $N \to \infty$.

The meaning of the symbols to be used in the build-up of the mathematical model can be found in the section as nomenclature.

2.1. Solutions for general boundary conditions

The following partial differential equation, describing drug undergoing diffusion in the $0 < \xi < 1$ interval and dissolution at

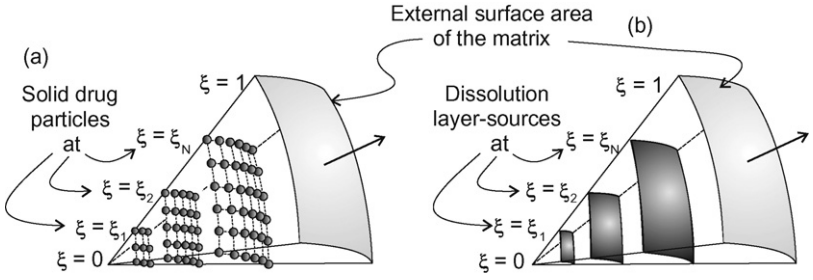

Fig. 2. (a) Three-dimensional schematic representation of spherical solid drug particles assembled on N cross-sectional areas arbitrarily located at ξ_1, ξ_2, and ξ_N into the matrix. (b) Representation in the continuum framework.

points $\xi_1, \xi_2, \ldots, \xi_N$, is a generalization of the mass balance equation formerly used for the planar geometry to all three simple geometries:

$$\frac{\partial}{\partial\tau}C(\xi,\tau) - \frac{1}{\xi^p}\frac{\partial}{\partial\xi}\left(\xi^p\frac{\partial}{\partial\xi}C(\xi,\tau)\right) = \sum_{n=1}^{N}\frac{1}{\xi^p}\delta(\xi-\xi_n)Pe_D\sigma(\xi)\alpha(\xi,\tau)[\,1-C(\xi,\tau)]$$

$$\text{in } 0<\xi<1, \quad \tau>0 \tag{1a}$$

$$\frac{\partial}{\partial\xi}C(\xi,\tau)=0 \quad \text{at } \xi=0, \quad \tau>0 \tag{1b}$$

$$\frac{\partial}{\partial\xi}C(\xi,\tau) = -Pe_B[C(\xi,\tau)-C_B(\tau)] \quad \text{at } \xi=1, \quad \tau>0 \tag{1c}$$

$$C(\xi,\tau)=C^0(\xi) \quad \text{for } \tau=0, \quad \text{in } 0\le\xi\ge 1 \tag{1d}$$

where exponent p depends on the geometry as follows:

$$p=\begin{cases}0 & \text{slab}\\ 1 & \text{cylinder}\\ 2 & \text{sphere}\end{cases} \tag{1e}$$

The depletion rate of the dimensionless surface area of the solid drug particles $\alpha(\xi_n,\tau)$, which are assumed to be spherical, is governed by the following set of ordinary differential equations (ODEs):

$$\frac{\mathrm{d}}{\mathrm{d}\tau}\alpha(\xi_n,\tau) = -2Pe_D\frac{L_c\,C_S}{r_n^0\rho_S}\alpha(\xi_n,\tau)^{1/2}[1-C(\xi_n,\tau)]$$

$$\text{for } \tau>0, \quad n=1,2,\ldots,N \tag{2a}$$

$$\alpha(\xi_n,\tau)=1 \quad \text{for } \tau=0, \quad n=1,2,\ldots,N \tag{2b}$$

which must be solved jointly with the boundary value problem given by Eqs. (1a), (1b), (1c) and (1d).

The model solution must be performed by numerical methods. For the same reasons argued in the previous contribution, we prefer to cast the original differential equations into equivalent integral equations to be numerically solved using an iteration scheme. Eqs. (1a), (1b), (1c) and (1d) are transformed to a single integral equation as follows: (i) Eq. (1a) is integrated with ξ^p as weight function and with Green's function $G(\xi,\tau;\bar{\xi},\bar{\tau})$ as test function to be defined in the following steps; (ii) an appropriate differential problem for Green's function is defined in a way of obtaining a suitable form of the integral solution; (iii) Green's function is identified by comparing the expression of the resulting integral solution with the corresponding generalized Fourier expansion; and finally, (iv) the associated eigenvalue problem is solved for each geometry. Since the procedure is similar to that applied in our previous contribution [34], we need not present details of the mathematical steps and will write only the resulting final expressions:

$$C(\xi,\tau) = \int_0^1 \mathrm{d}\bar{\xi}\,\bar{\xi}^p G(\xi,\tau;\bar{\xi},0)C^0(\bar{\xi}) + Pe_B\int_0^\tau \mathrm{d}\bar{\tau}\,G(\xi,\tau;1,\bar{\tau})C_B(\bar{\tau}) + Pe_D\int_0^\tau \mathrm{d}\bar{\tau}\sum_1^N G(\xi,\tau;\xi_n,\bar{\tau})\sigma^0(\xi_n)\alpha(\xi_n,\bar{\tau}) \times[1-C(\xi_n,\bar{\tau})] \quad \text{for } N=\text{finite} \tag{3a}$$

and

$$C(\xi,\tau) = \int_0^1 \mathrm{d}\bar{\xi}\,\bar{\xi}^p G(\xi,\tau;\bar{\xi},0)C^0(\bar{\xi}) + Pe_B\int_0^\tau \mathrm{d}\bar{\tau}\,G(\xi,\tau;1,\bar{\tau})C_B(\bar{\tau}) + Pe_D\int_0^\tau \mathrm{d}\bar{\tau}\int_0^1 \mathrm{d}\bar{\xi}\,G(\xi,\tau;\bar{\xi},\bar{\tau})\varphi^0(\bar{\xi})\alpha(\bar{\xi},\bar{\tau}) \times[1-C(\bar{\xi},\bar{\tau})] \quad \text{for } N\to\infty \tag{3b}$$

where Green's function is the following Fourier expansion:

$$G(\xi,\tau;\bar{\xi},\bar{\tau}) = \sum_0^\infty \exp[-\beta_m^2(\tau-\bar{\tau})]\psi_m^{-1}\phi_m(\xi)\phi_m(\bar{\xi})\Theta(\tau-\bar{\tau}) \tag{4}$$

Table 1 summarizes the auxiliary problem to be satisfied by Green's function and the associated eigenvalue problem. Table 2 resumes the eigenvalues β_m, the eigenfunctions $\phi_m(\xi)$, and the norms Ψ_m, to be used for the calculation of Green's functions for planar, cylindrical and spherical geometries. The details to solve the eigenvalue problem for each geometrical shape can be found elsewhere [35]. It is noticeable that the eigenvalues only depend on the value of Pe_B, so that once they are calculated they simply form a data file to be used for the numerical solution whichever

Table 1
Auxiliary problem defining of Green's function and the associated eigenvalue problem

Green's function
$\frac{\partial}{\partial\bar{\tau}}G(\xi,\tau;\bar{\xi},\bar{\tau}) + \frac{1}{\bar{\xi}^p}\frac{\partial}{\partial\bar{\xi}}\left(\bar{\xi}^p\frac{\partial}{\partial\bar{\xi}}G(\xi,\tau;\bar{\xi},\bar{\tau})\right) =$
$-\frac{1}{\bar{\xi}^p}\delta(\xi-\bar{\xi})\delta(\tau-\bar{\tau})$ in $0<\bar{\xi}<1$, for $\tau>0$
$\frac{\partial}{\partial\bar{\xi}}G(\xi,\tau;\bar{\xi},\bar{\tau})=0$ at $\xi=0$, $\tau>0$
$\frac{\partial}{\partial\bar{\xi}}G(\xi,\tau;\bar{\xi},\bar{\tau}) + Pe_BG(\xi,\tau;\bar{\xi},\bar{\tau})=0$ at $\xi=1$, $\tau>0$
$G(\xi,\tau;\bar{\xi},\tau+\varepsilon)=0$ for $\varepsilon>0$, in $0<\bar{\xi}<1$, where ε is a small but not zero positive number
Eigenvalue problem
$\frac{1}{\xi^p}\frac{\mathrm{d}}{\mathrm{d}\xi}\left(\xi^p\frac{\mathrm{d}}{\mathrm{d}\xi}\phi_m(\xi)\right) + \beta_m^2\phi_m(\xi)=0$ in $0<\bar{\xi}<1$
$\frac{\mathrm{d}}{\mathrm{d}\xi}\phi_m(\xi)=0$ at $\xi=0$
$\frac{\mathrm{d}}{\mathrm{d}\xi}\phi_m(\xi) + Pe_B\phi_m(\xi)=0$ at $\xi=1$
Orthogonality condition
$\int_0^1 \mathrm{d}\bar{\xi}\,\bar{\xi}^p\phi_n(\bar{\xi})\phi_m(\bar{\xi}) = \delta_{nm}\psi_m$, where δ_{nm} is the Kronecker delta

Table 2
Solutions of the eigenvalue problem associated with Green's function for the general boundary conditions given by Eqs. (1b) and (1c)

Form of the matrix	p	Eigenfunctions $\phi_m(\xi)$	Norm ψ_m^{-1}	Eigenvalues β_m are real positive roots of
Planar	0	$\cos\beta_m\xi$	$2(\beta_m^2+Pe_B^2)/(\beta_m^2+Pe_B^2+Pe_B)$	$-\beta_m\tan\beta_m+Pe_B=0$
Cylindrical[a]	1	$J_0(\beta_m\xi)$	$(2/J_0^2(\beta_m))(\beta_m^2/(Pe_B^2+\beta_m^2))$	$-\beta_m J_1(\beta_m)+Pe_B J_0(\beta_m)=0$
Spherical	2	$(\sin\beta_m\xi)/\xi$	$2(\beta_m^2+(Pe_B-1)^2)/(\beta_m^2+(Pe_B-1)^2+Pe_B-1)$	$\beta_m\cot\beta_m+Pe_B-1=0$

[a] J_0 and J_1 are the Bessel functions of first kind of order zero and one, respectively.

the parameters characterizing the dissolution process. It should be noted that $\sigma^0(\xi_n)$ is the initial overall surface area of the solid drug at $\xi=\xi_n$ per external surface area unit matrix, while $\varphi^0(\xi)$ is the initial overall surface area of solid drug at ξ per volume unit matrix ($cm^2\,cm^{-3}$), as defined in nomenclature.

It is noteworthy that Eq. (3b), which arises from Eq. (3a) as asymptotic case as $N\to\infty$, is precisely the solution of the diffusion equation with the Noyes–Whitney equation as continuum dissolution source in the $0<\xi<1$ interval (see Appendix A). Eq. (3a) allows the treatment of spatially continuous or piecewise continuous loading of dissolved drug by setting $C^0(\xi)$, including discontinuous solid drug loading and arbitrary particle size distributions by specifying $\sigma^0(\xi_n)$ and r_n^0, as desired. Eq. (3b) is suitable to analyze release systems with evenly and arbitrarily dissolved and/or dispersed solid drug into the whole matrix, according to $C^0(\xi)$ and/or $\varphi^0(\xi)$. These features render a great flexibility of both integral equations to handle different architectures of release systems.

To complete the integral formulation of the mathematical model, a straightforward integration of the set of ODEs described by Eqs. (2a) and (2b) gives:

$$\alpha(\xi_n,\tau)=1-2Pe_D\frac{L_c\,C_S}{r_n^0\rho_S}\int_0^\tau d\bar\tau\,\alpha(\xi_n,\bar\tau)^{1/2}[1-C(\xi_n,\bar\tau)]$$
$$\text{for } n=1,2,\ldots,N,\quad \tau>0 \tag{5a}$$

and

$$\alpha(\xi,\tau)=1-2Pe_D\frac{L_cC_S}{r^0(\xi)\rho_S}\int_0^\tau d\bar\tau\,\alpha(\xi,\bar\tau)^{1/2}[1-C(\xi,\bar\tau)]$$
$$\text{for } N\to\infty,\quad \tau>0 \tag{5b}$$

which must be solved by coupling to Eqs. (3a) or (3b).

2.2. Solutions for the perfect sink condition

The perfect sink condition is a simplifying assumption widely used in the modeling of drug release. To deal with this special boundary condition, $Pe_B=\infty$ and $C_B=0$ must be settled into the second integral term of Eqs. (3a) and (3b), but this is not directly possible. This drawback can be circumvented following a three-step procedure [35]: (i) $Pe_B G(\xi,\tau;1,\bar\tau)$ is replaced by $-\partial G(\xi,\tau;\bar\xi,\bar\tau)/\partial\bar\xi$ evaluated at $\bar\xi=1$, as established by the outer boundary condition in the auxiliary problem defining Green's function (Table 1); (ii) Green's function is taken as the solution of that auxiliary problem subjected to $G(\xi,\tau;1,\bar\tau)=0$ as modified boundary condition; and (iii) C_B is assumed to be equal to zero at all times.

After proceeding as aforementioned, Eqs. (3a) and (3b) reduce to:

$$C(\xi,\tau)=\int_0^1 d\bar\xi\,\bar\xi^p G(\xi,\tau;\bar\xi,0)C^0(\bar\xi)$$
$$+Pe_D\int_0^\tau d\bar\tau\sum_1^N G(\xi,\tau;\bar\xi_n,\bar\tau)\sigma^0(\xi_n)\alpha(\xi_n,\bar\tau)$$
$$\times[1-C(\xi_n,\bar\tau)]\quad\text{for } N\to\text{finite} \tag{6a}$$

and

$$C(\xi,\tau)=\int_0^1 d\bar\xi\,\bar\xi^p G(\xi,\tau;\bar\xi,0)C^0(\bar\xi)$$
$$+Pe_D\int_0^\tau d\bar\tau\int_0^1 d\bar\xi\,G(\xi,\tau;\bar\xi,\bar\tau)\varphi^0(\bar\xi)\alpha(\bar\xi,\bar\tau)$$
$$\times[1-C(\bar\xi,\bar\tau)]\quad\text{for } N\to\infty \tag{6b}$$

which are the respective solutions for the perfect sink condition. Table 3 summarizes the expressions for $\phi_m(\xi)$, β_m, and Ψ_m to be used for computing Green's functions for all three geometries.

3. Computational method

3.1. Numerical algorithm

As reported in the previous contribution, the numerical method proceeds at increasing values of time following an iteration scheme according to the sequence [34]. Solution to the integral equations is then being sought using Piccard's successive approximations:

$$C(\xi_n,\tau)^{k+1}=F[C(\xi_n,\tau)^k]\quad\text{for } n=1,2,\ldots,N,\quad\tau>0 \tag{7a}$$

Table 3
Solutions of the eigenvalue problem associated with Green's function for the perfect sink condition

Form of the matrix	p	Eigenfunctions $\phi_m(\xi)$	Norm ψ_m^{-1}	Eigenvalues β_m are real and positive roots of
Planar	0	$\cos\beta_m\xi$	2	$\beta_m=(2m+1)\pi/2$
Cylindrical[a]	1	$J_0(\beta_m\xi)$[b]	$2/J_1^2(\beta_m)$[b]	$J_0(\beta_m)=0$[b]
Spherical	2	$(\sin\beta_m\xi)/\xi$	2	$\beta_m=m\pi$

[a] J_0 and J_1 are the Bessel functions of first kind of order zero and one, respectively.

[b] $\beta_0=0$ is also an eigenvalue, then the corresponding eigenfunction is $\phi_0=1$, and the norm $\psi_m^{-1}=2$.

and

$$C(\xi,\tau)^{k+1} = F[C(\xi,\tau)^k] \quad \text{for } N \to \infty, \quad \tau > 0 \tag{7b}$$

where F represents the R.H.S. of Eqs. (3a), (3b), (6a) and (6b), and superscript k denotes kth iteration. This sequence converges to the solution if the Lipzchitz condition is satisfied [36]. The convergence can be usually achieved for values of the parameters typically found in dissolution/diffusion-controlled drug release from planar matrices, but an unexpected numerical instability arises under certain conditions for non-planar geometry, as shown below.

A significant improvement of the numerical performance was reached combining the above iteration scheme with the homotopy method according to:

$$C(\xi_n,\tau)^{k+1} = (1-s)C(\xi_n,\tau)^k + sF[C(\xi_n,\tau)^k] \quad \text{for } n = 1,2,\ldots,N, \quad \tau > 0 \tag{8a}$$

and

$$C(\xi,\tau)^{k+1} = (1-s)C(\xi,\tau)^k + sF[C(\xi,\tau)^k] \quad \text{for } N \to \infty, \quad \tau > 0 \tag{8b}$$

where auxiliary parameter s is defined into the $0 \le s \le 1$ interval [37–40]. The homotopy path begins with $s = 0$ and finishes with $s = 1$. Note that when s is unity, Eqs. (8a) and (8b) reduce to Eqs. (7a) and (7b), thus satisfying the original solution.

In order to illustrate the advantages of this refined numerical procedure, Fig. 3 shows the cumulative and rate profiles of drug released from cylindrical and spherical matrices of two-layer architecture for a case exhibiting the aforementioned instability. For both geometries, numerical simulation based on the classical scheme without homotopy gives divergent results at longer times for the cylinder (black region) and the sphere (gray region). However, the convergence was always achieved using the iteration scheme with homotopy (solid lines). This numerical refinement was then used unless otherwise specified.

3.2. Numerical calculations

All calculations were performed using FORTRAN programmes in double precision arithmetic. Eigenvalues β_m were found as positive roots of non-linear equations using Müller's method for the case of cylindrical geometry [41], and Brent's method for the planar and spherical geometries [42]. The Bessel functions of the first kind of order zero and order one were evaluated using standard routines. It was numerically determined that the first twenty eigenvalues are enough to accurately compute Green's functions. A simple equally spaced quadrature algorithm based on the Newton 3/8 method was used to perform the numerical integration [43]. The iterative processes were carried out until the relative errors of the calculated values were found to be smaller than 10^{-4}. The total number of grid points used in the ξ- and τ-coordinates depended upon Pe_B and Pe_D values. The higher are the values of the Peclet numbers, the greater the need for more refined grids. However, highly refined grids would prohibitively demand computer memory space and running time. The results obtained with different grid sizes were compared to those accepted as the exact solution, which was achieved with 500 grid points. After extensive numerical work, it was concluded that 100–150 grid points render a good agreement with the exact solution.

3.3. Numerical exploration

For all calculations presented herein, the effect of the rate-limiting step on the release patterns was studied by varying the Pe_D value from 0.1 (dissolution-controlled regime) to 1 (dissolution/diffusion-controlled regime). Likewise, the effect of the external mass transport resistance was analyzed by changing the Pe_B value from 10 (non-negligible resistance) to 100 (negligible resistance). Diverse matrix systems were designed keeping constant the surface area to volume ratio and in order to give approximately the same total drug release. Accordingly, that ratio was assumed to be equal 10, and the surface area 1 cm^2, for all three geometries. Thus, the resulting half-thickness or radius

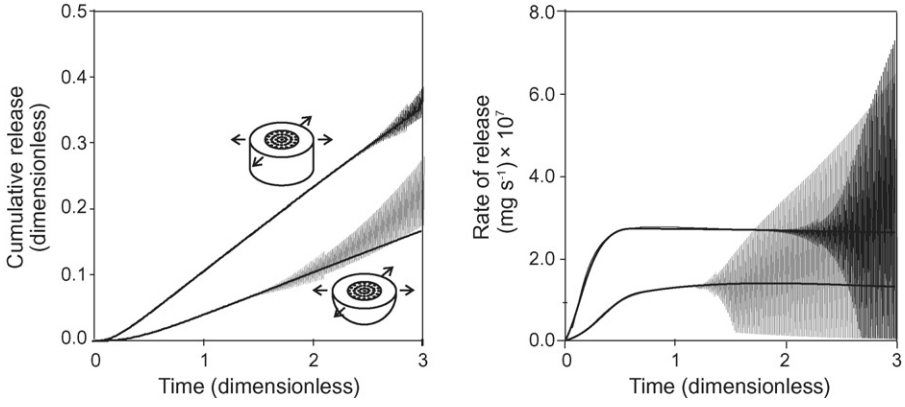

Fig. 3. Cumulative and rate of drug release profiles, as a function of the dimensionless time, for two-layer matrix systems of cylindrical and spherical geometry. Black and gray regions show divergent results resulting from the iteration scheme without homotopy according to Eqs. (7a) and (7b). Solid lines show convergent results obtained using the iteration scheme combined with homotopy according to Eqs. (8a) and (8b). The calculations were performed for a solid drug loading of 2% (w/v) loaded into the inner layer: $C^0_{outer} = \varphi^0_{outer} = 0$, $C^0_{inner} = 1$ and $\varphi^0_{inner} = 0.02$; drug particle diameter of 5 μm; $C_B = 0$; $L_c = 0.1$ cm; $D = 1 \times 10^{-8}$ cm^2 s^{-1}; $C_S = 5$ mg cm^{-3}; $\rho_S = 1.4$ g cm^{-3}; $Pe_B = 100$; $Pe_D = 1$.

L was 0.1, 0.2, and 0.3 cm for the slab, the cylinder and the sphere, respectively. Note that the characteristic length L_c was equal to 0.1 cm for the all three geometries. Solid drug loadings ranging from 0 to 5% (w/v), and particle sizes from 1 to 10 μm in diameter, were examined. Since the solid drug particles are assumed to be spherical, the initial solid drug surface per unit cross-sectional area $\sigma^0(\xi_n)$ was readily determined from the initial particle size and solid drug loading at each drug dissolution source. Both continuous and piecewise continuous drug distributions were chosen to show how different architectures, including single-layer and multi-layer matrix systems, can be readily handled within this mathematical framework.

4. Numerical results and discussion

Some examples illustrating the usefulness of the integral method for solving the design equations of dissolution and dissolution/diffusion-controlled drug release from planar, cylindrical and spherical matrices of quite different architectures will be presented. However, before doing so we will examine the quality of the mathematical and numerical solutions.

4.1. Comparison with previous analytical solutions

Unfortunately, no exact comparison formulas for testing the full descriptive potential of the derived integral equations are available. Analytical solutions for the simplest case of uniformly dissolved drug into the whole matrix and perfect sink condition are only feasible to be compared. To this special case, after integration, Eq. (6b) gives the following mathematical expressions for the cumulative release:

$$Q(\tau) = 1 - \frac{8}{\pi^2}\sum_{n=0}^{\infty}\frac{1}{(2n+1)^2}\exp\left[-(2n+1)^2\left(\frac{\pi^2}{4}\right)\tau\right]$$

$$\text{for slab } (p=0) \tag{9}$$

$$Q(\tau) = 1 - 4\sum_{n=1}^{\infty}\frac{1}{\beta_n^2}\exp[-\beta_n^2\tau] \quad \text{for cylinder } (p=1) \tag{10}$$

$$Q(\tau) = 1 - \frac{6}{\pi^2}\sum_{n=1}^{\infty}\frac{1}{n^2}\exp[-n^2\pi^2\tau] \quad \text{for sphere } (p=2) \tag{11}$$

which are those given by Crank [44].

4.2. Comparison with previous analytical approximations

Analytical short-time approximations for the fraction of released drug have been developed to facilitate the analysis of the early stages of the release process of a slowly dissolving drug from planar and spherical matrix systems [31,32]. Then, the results from these integral equations were compared with those from such analytical approximations. The comparison was performed for uniform solid drug loading largely exceeding the amount of dissolved drug and the sink condition. Fig. 4 depicts the fraction of released drug as a function of the square root of the time. For both geometries, at earlier stages is evidenced a close match between the predictions from the integral equations presented in this work (solid lines) and the approximations by Frenning (dash lines). As expected, the discrepancy between the predictions increases at larger stages because the analytical approximations are no longer applicable.

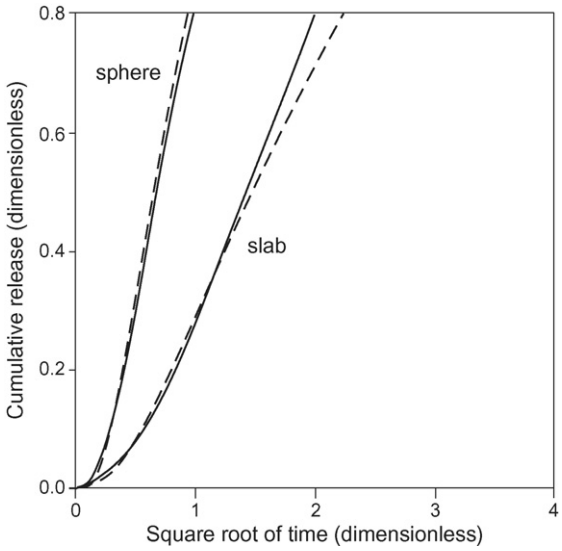

Fig. 4. Comparison between the fractions of released drug, as a function of the square root of time, calculated according to the model prediction (—) and the short-time approximations given by Frenning (– – –) for planar and spherical single-matrix systems. The calculations were performed for a solid drug loading of 5% (w/v) uniformly distributed into the single-matrix, drug particle diameter of 10 μm; $C_B = 0$; $L_c = 0.1$ cm; $D = 1 \times 10^{-8}$ cm^2 s^{-1}; $C_S = 5$ mg cm^{-3}; $C^0 = 1$; $\rho_S = 1.4$ g cm^{-3}; $Pe_B = 100$; $Pe_D = 1$.

4.3. Numerical validation of special cases

It was numerically corroborated how by increasing N, the solution given by general Eq. (3a) progressively approximates that provided by Eq. (6a). Simulations were performed for a constant dosage of solid drug increasingly dispersed into the matrix by decreasing the drug loading at the dissolution layer-sources, in favor of an increased number of these. Fig. 5 shows the resulting drug profiles as a function of the ξ-coordinate, at various time intervals, for $Pe_D = 1$ and $Pe_B = 100$. Note that the profiles for four (short dash line), seven (dash dot line), and 24 (dash line) dissolution layer-sources progressively match with those for a continuum dissolution source, as expected. Undulating profiles having a maximum in the neighborhoods of each source are obtained when the solid drug loading is distributed into a small number of dissolution layer-sources. Physically, these undulations are a consequence of the dissolution/diffusion-controlled regime, the diffusion rate being quite slow for equalizing the concentration profiles of dissolved drug between the large diffusion lengths separating the dissolution layer-sources. Then, the profiles begin to be smoothed as soon as the dissolution sources are successively exhausted from the outer boundary inwards. The undulations are smoothed when an increased number of sources are settled, and obviously vanish when the dissolution sources become continuum. For $Pe_B = 100$ and $Pe_D = 0.1$, whichever the

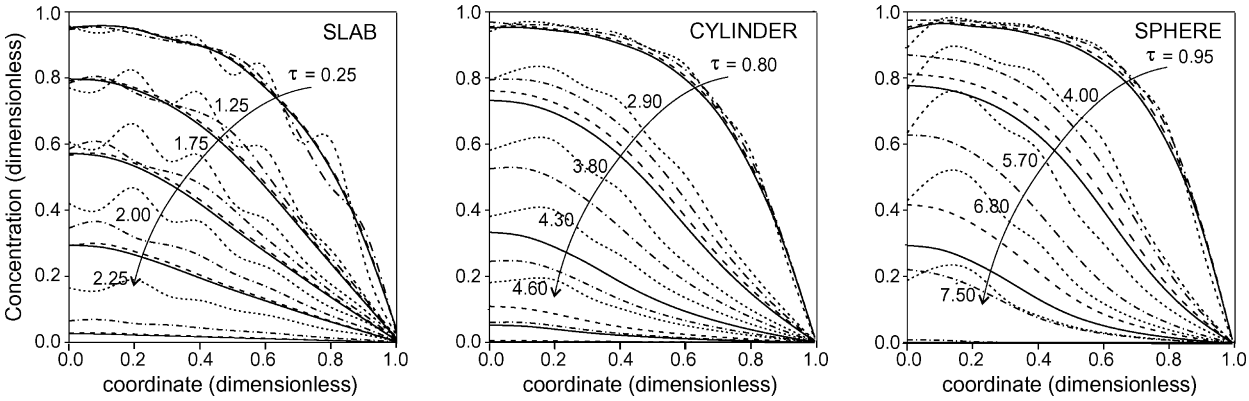

Fig. 5. Drug concentration profiles as a function of the dimensionless spatial coordinate, at various time intervals, for a solid drug loading of 2% (w/v) spatially distributed into four (- - -), seven (–·–·–), and 24 (– – –) dissolution layer-sources. Solid lines correspond to the solution of the diffusion equation with a continuum dissolution source described by the Noyes–Whitney equation (—). The calculations were performed for a particle diameter of 5 μm; $C_B = 0$; $L_c = 0.1$ cm; $D = 1 \times 10^{-8}$ cm^2 s^{-1}; $C_S = 5$ mg cm^{-3}; $C^0 = 1$; $\rho_S = 1.4$ g cm^{-3}; $Pe_B = 100$; $Pe_D = 1$.

number of dissolution layer-sources, all concentration profiles (not shown) are equally smoothed due to a diffusion rate faster than the dissolution rate.

It was also numerically tested how by increasing the value of Pe_B, and by setting $C_B = 0$, the solution of general Eq. (3b) approaches that of Eq. (6b). Fig. 6 shows how the drug concentration profiles calculated for $Pe_B = 10$ and $C_B = 0$ (dash line) differ from those given for the perfect sink condition but the results match for $Pe_B = 100$ (dash dot line). Thus, for practical purposes, the values obtained from Eq. (3b) for $Pe_B \geq 100$ and $C_B = 0$ can be used as the solution for the perfect sink condition.

The above-described numerical behaviors are congruous with those mathematically demonstrated as asymptotic cases. This feature can be used as another indicator confirming the quality of both mathematical and numerical solutions.

4.4. Example calculations for single-layer matrix systems

Fig. 7 illustrates the rate of release, cumulative release, and the surface area of the solid drug particles as a function of the dimensionless time for solid drug particles uniformly dispersed into single-layer matrix systems approaching the perfect sink condition, $Pe_B = 100$. Results for $Pe_D = 1$ and 0.1 are included for the all three geometries. The dissimilar release patterns can be ascribed to the inherent geometrical parameters, as well as to the Pe_D value. Obviously, dependence of the matrix cross-sectional area with the diffusion length is zero for the slab ($p = 0$), linear for the cylinder ($p = 1$), and quadratic for the sphere ($p = 2$). Moreover, the ratio between the surface area and volume of the matrix was assumed to be constant for all three geometries. Therefore, the greatest diffusion length in the sphere is three times greater than that of the slab. Likewise, this length in the cylinder is two times greater than that of the slab. These coupled geometrical effects determine that the planar matrix exhibits a greater flux compared with those of non-planar geometry, that of the sphere being the lowest one. Hence, the depletion rate of the solid drug particles is the fastest into the slab and the slowest one into the sphere. Furthermore, the lower is the Pe_D value, the slower the drug dissolution rate, and the higher the relative rate of diffusion. For dissolution–diffusion-controlled regime, $Pe_D = 1$, the slab exhibits a release pattern having three well-defined stages. At the early stages, the release rate declines quickly until the solid drug particles begin to vanish. Then, a slower decline takes place while the vanishing process advances from the boundary inwards until the solid drug completely vanishes.

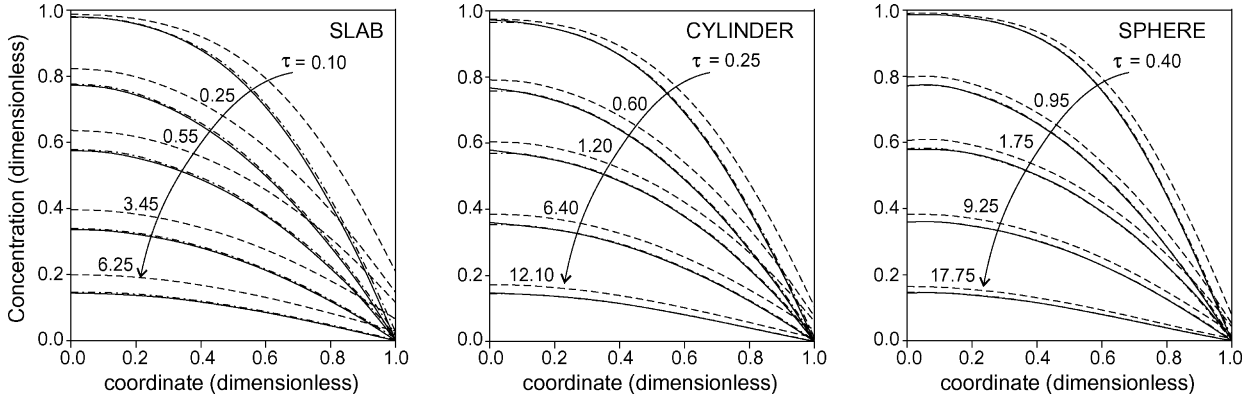

Fig. 6. Drug concentration profiles as a function of the dimensionless spatial coordinate, at various time intervals, for a solid drug loading of 2% (w/v) uniformly distributed into the single-matrix, for $C_B = 0$; $Pe_D = 1$; $Pe_B = 10$ (- - -); $Pe_B = 100$ (–·–·–); and the perfect sink condition (—). The calculations were performed for a particle diameter of 5 μm; $L_c = 0.1$ cm; $D = 1 \times 10^{-8}$ cm^2 s^{-1}; $C_S = 5$ mg cm^{-3}; $C^0 = 1$; $\rho_S = 1.4$ g cm^{-3}.

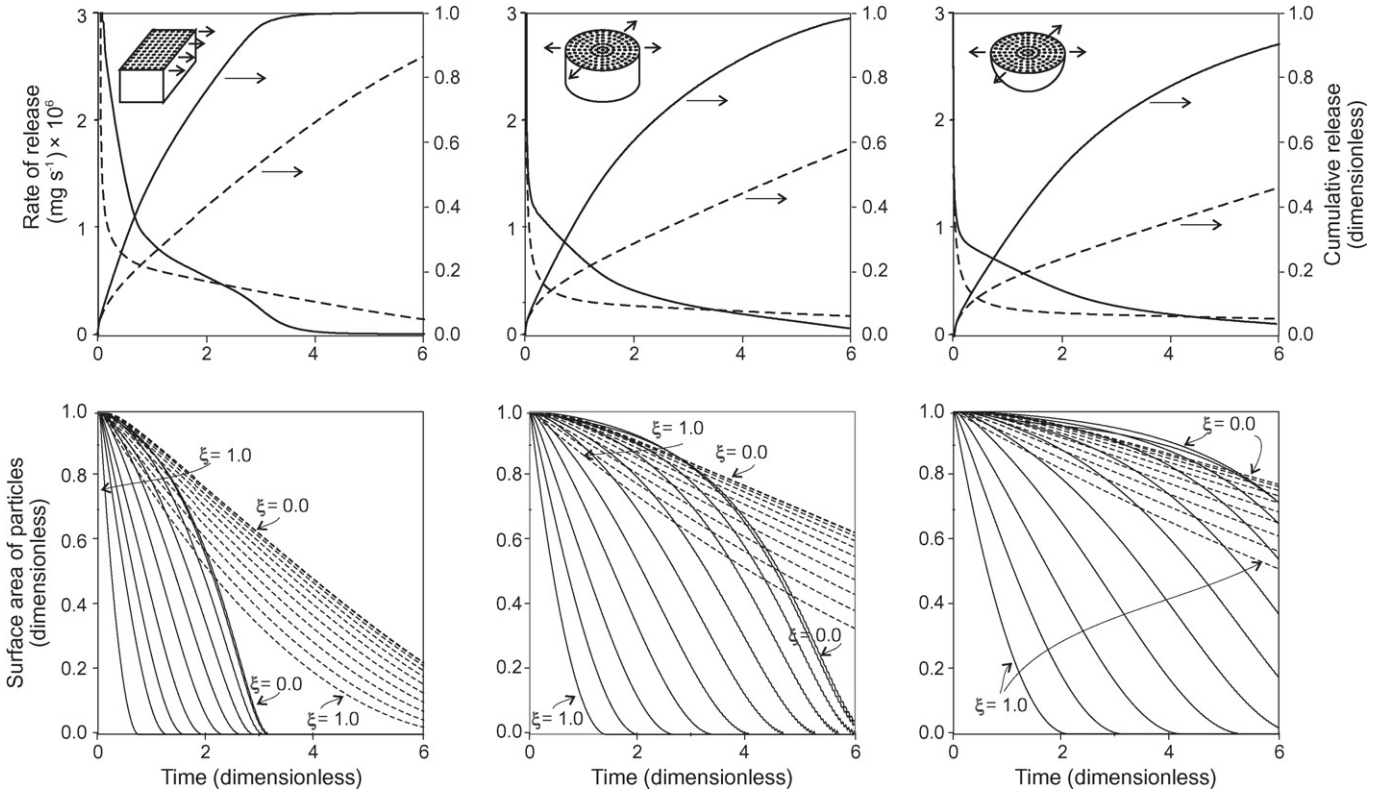

Fig. 7. Rate of drug release, cumulative release, and the surface area of the solid drug particles, as a function of time, for a solid drug loading of 2% (w/v) uniformly distributed into a single-layer matrix. The calculations were performed for a particle diameter of 5 μm; $C_B = 0$; $L_c = 0.1$ cm; $D = 1 \times 10^{-8}$ cm^2 s^{-1}; $C_S = 5$ mg cm^{-3}; $C^0 = 1$; $\rho_S = 1.4$ g cm^{-3}; $Pe_B = 100$; $Pe_D = 1$ (—); $Pe_D = 0.1$ (– – –). $\xi = 0.0$ and 1.0 denote the inner and outer boundaries of the matrix region containing solid drug particles, respectively.

Finally, a faster loss in release rate occurs until all remaining dissolved drug is released. This latter stage is neither exhibited for the cylinder nor the sphere because none of the solid drug particles can be exhausted within the simulated time. For dissolution-controlled regime, $Pe_D = 0.1$, burst effects display shorter periods and steeper profiles. This is due to the fact that the slower drug dissolution process is unable to sustain the faster diffusion release of the dissolved drug at the early stages. In this case, the depletion rates of the solid drug particles are quite uniform since the impulsive force for the dissolution process is equalized into the matrix by the relative faster drug diffusion transport. Thus, after burst effects, a narrow size distribution of dissolving solid drug particles yields reduced release rates exhibiting plateau values. Note that for short times in the region closest to the center of the matrix, the dimensionless surface areas of the solid drug particles are larger for $Pe_D = 1$ than for $Pe_D = 0.1$. It appears to be a somewhat paradoxical result, but this behavior can be explained as follows. At the beginning of the dissolution/diffusion-controlled release, marked concentration gradients of dissolved drug are established into the matrix region closer to the external boundary. This fact determines that the dissolution and exhaustion processes of the solid drug particles begin and progress from the outer boundary inwards the matrix. Consequently, the most external particles quickly decline, while the most internal ones remain almost unchanged. On the other hand, under dissolution-controlled release the depletion rates of the solid drug particles are quite uniform since the impulsive force for the dissolution process is equalized into the whole matrix as aforementioned. Therefore, the size of the dissolving particles reduces more uniformly under this controlling regime than for the dissolution/diffusion-controlled release. This behavior determines the presence of smaller particles for $Pe_D = 0.1$ than for $Pe_D = 1$, within the region closest to the center of the matrix. The differences in size are more evident in the sphere than in the cylinder due to the effect of the geometry on the drug diffusion process.

Integral Eqs. (3b) and (6b) can also be used to predict the effects of spatially non-uniform drug loading on the drug release patterns by setting the desired functionalities of $C^0(\xi)$ and $\varphi^0(\xi)$. We will not present this type of analysis due to the practical limits on loading a monolithic matrix with non-uniform drug distribution [24]. In preference, the flexibility of the integral method for handling piecewise continuous distributions of drug resembling multi-layer systems of the same matrix material will be ascertained since the technology for these systems is available.

4.5. Example calculations for two-layer matrix systems

Composite matrices consisting of two layers of equal diffusivity can be simulated by incorporating the following piecewise continuous distributions of dissolved and undissolved drug into our framework:

$$C^0(\xi) = \Theta(\xi^* - \xi)C^0_{\text{inner}}(\xi) + \Theta(\xi - \xi^*)C^0_{\text{outer}}(\xi) \tag{12a}$$

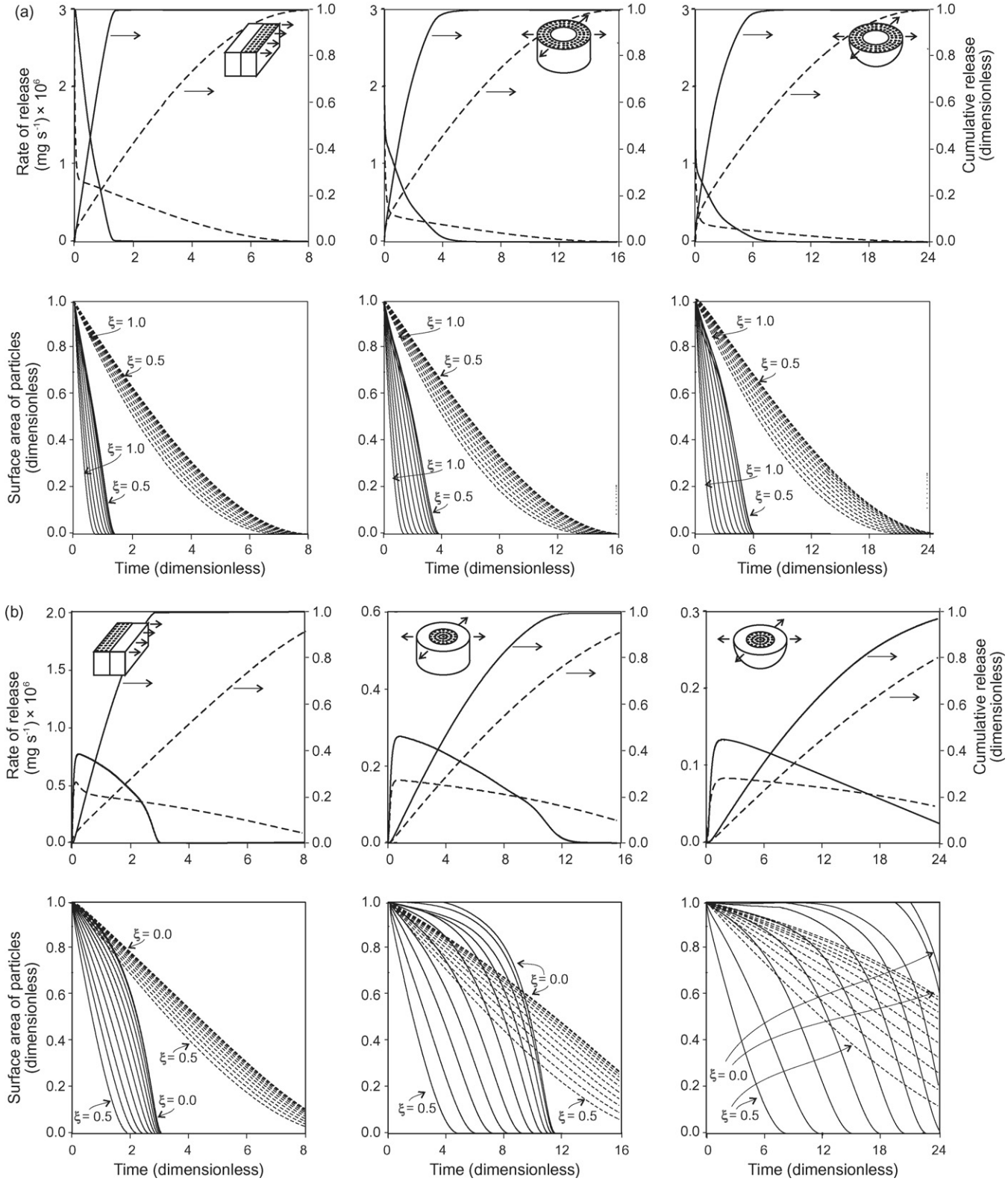

Fig. 8. Rate of drug release, cumulative release, and the surface area of the solid drug particles, as a function of time, for a solid drug loading dissimilarly distributed in two layers of the same thickness, $\xi^* = 0.5$. (a) All the drug loaded into the outer layer: $C^0_{\text{outer}} = 1$ and $\varphi^0_{\text{outer}} = 0.02$, $C^0_{\text{inner}} = \varphi^0_{\text{inner}} = 0$. $\xi = 0.5$ and 1.0 denote the inner and outer boundaries of the matrix region containing solid drug particles, respectively. (b) All the drug loaded into the inner layer: $C^0_{\text{outer}} = \varphi^0_{\text{outer}} = 0$, $C^0_{\text{inner}} = 1$ and $\varphi^0_{\text{inner}} = 0.02$. $\xi = 0.0$ and 0.5 denote the inner and outer boundaries of the matrix region containing solid drug particles, respectively. The calculations were performed for solid drug loading of 2% (w/v); drug particle diameter = 5 μm; $C_B = 0$; $L_c = 0.1$ cm; $D = 1 \times 10^{-8}$ cm^2 s^{-1}; $C_S = 5$ mg cm^{-3}; $\rho_S = 1.4$ g cm^{-3}; $Pe_B = 100$, $Pe_D = 1$ (—); $Pe_D = 0.1$ (– – –).

$$\varphi^0(\xi) = \Theta(\xi^* - \xi)\varphi^0_{\text{inner}}(\xi) + \Theta(\xi - \xi^*)\varphi^0_{\text{outer}}(\xi) \quad (12b)$$

which, by virtue of the Heaviside unit step function Θ, become:

$$C^0(\xi) = \begin{cases} C^0_{\text{inner}}(\xi) & 0 < \xi < \xi^* \\ C^0_{\text{outer}}(\xi) & \xi^* < \xi < 1 \end{cases} \quad (13a)$$

$$\varphi^0(\xi) = \begin{cases} \varphi^0_{\text{inner}}(\xi) & 0 < \xi < \xi^* \\ \varphi^0_{\text{outer}}(\xi) & \xi^* < \xi < 1 \end{cases} \quad (13b)$$

where ξ^* is the dimensionless thickness of the inner layer. Thus, different two-layer architectures can be undertaken by selecting C^0_{inner}, C^0_{outer}, φ^0_{inner}, φ^0_{outer}, and ξ^* in a way of simulating the desired architecture. Some specific examples will be presented.

Fig. 8a and b depicts the rate of release, cumulative release, and the surface area of the solid drug particles as a function of the dimensionless time for $Pe_D = 1$ and 0.1, $Pe_B = 100$, and a solid drug loading of 2% (w/v) dissimilarly distributed in two layers of equal thickness. When the drug is loaded into the outer layer (Fig. 8a), keeping the inner one empty, the release rate-controlling regime and geometry affect the drug release patterns. The differences are clearly observable during the early stages of the process. For the dissolution/diffusion-controlled regime, $Pe_D = 1$, the release rate of drug from the slab steadily diminishes until all solid drug particles rapidly vanish, yielding a relatively short drug release period in comparison with the non-planar geometries. However, after burst effects, a more sustained release is attainable for the cylinder and the sphere, but without approaching constant release rates. For the dissolution-controlled regime, $Pe_D = 0.1$, more sustained and reduced release rates are feasible of being achieved for all three geometries, but also the undesirable burst effect cannot be avoided. Conversely, when the drug is loaded into the inner layer only (Fig. 8b), acting the outer one as a membrane, a time-delayed release occurs instead of the burst effect. This effect is due to the drug must be transferred to the initially empty outer layer, and definitely increases in the order slab < cylinder < sphere. The same remarks also apply to the decline of the drug release rate. Both features are attributable to the above-mentioned geometrical factors. Unlike the case of drug loaded into the outer layer, sustained release rates are also possible to be reached for $Pe_D = 1$, displaying how drug distribution changes significantly modify the release pattern. The plots displaying the depletion of the dimensionless surface area of solid drug particles give a further insight to explain the release patterns. Note that the depletion rate of drug particles depends on both their position into the matrix and the release rate-controlling regime. The greater is the proximity to the outer boundary, the faster the depletion rate. The slower is the drug dissolution rate, the lower the position effect on the depletion rate. Consequently, the surface area of the drug particles decreases uniformly throughout the matrix under

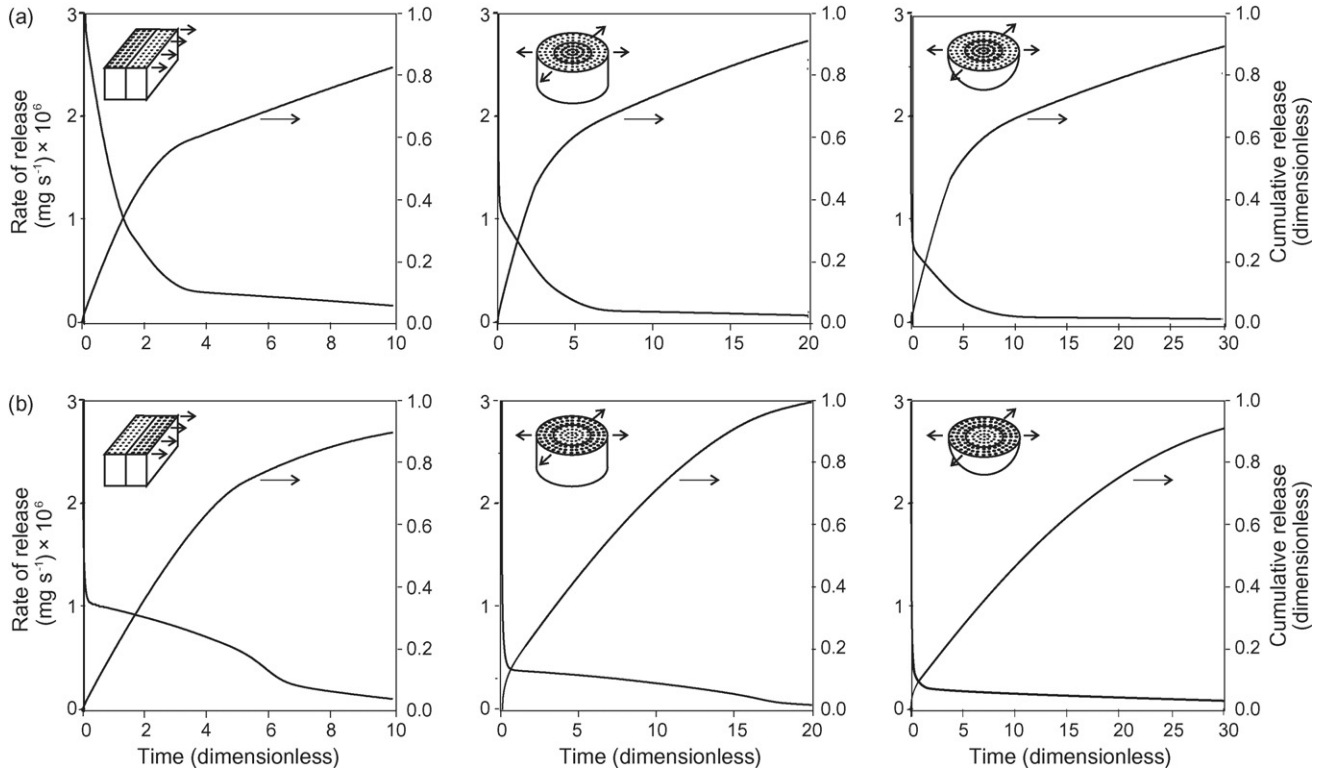

Fig. 9. Rate of drug release and cumulative release, as a function of time, for a total solid drug loading of 5% (w/v) equally distributed in two layers of the same thickness, $\xi^* = 0.5$, $C^0_{\text{inner}} = C^0_{\text{outer}} = 1$ and $\varphi^0_{\text{inner}} = \varphi^0_{\text{outer}} = 0.025$. (a) Drug particles of 10 and 1 μm in the inner and outer layers, respectively. (b) Drug particles of 1 and 10 μm in the inner and outer layers, respectively. The calculations were performed for $C_B = 0$; $L_c = 0.1$ cm; $D = 1 \times 10^{-8}$ cm^2 s^{-1}; $C_S = 5$ mg cm^{-3}; $\rho_S = 1.4$ g cm^{-3}; $Pe_B = 100$; $Pe_D = 0.1$.

dissolution-controlled regime, resulting in sustained release patterns increasing the order slab < cylinder < sphere. Otherwise, under dissolution/diffusion-controlled regime, the drug particles undergo depletion at different rates depending on whether they are located into the matrix, yielding an invariable decline of the release rate that hinders sustained drug release. It is again noteworthy the effect of the geometry on the release rate, and therefore over the matrix lifetime.

Fig. 9a and b illustrates how varying the drug particle size distribution changes the release pattern. Indeed, simulation results are shown for dissolution-controlled drug release from symmetric matrices having two layers of equal thickness, containing the same solid drug loading but different drug particle sizes. When the inner and outer layers are initially loaded with particles of 10 and 1 μm, respectively (Fig. 9a), the fine particles into the outer layer vanish long before those of larger size into the inner layer. Thus, after burst effect, the release rate of drug from the slab slowly decreases until the complete exhaustion of fine particles is achieved. Then, the release rate declines still more while the large particles dissolve into the inner layer. Non-planar geometries exhibit slower release rates, delaying the described transition and extending the drug release periods. Note that the release profiles are illustrated for different time scales depending on the geometrical shapes. A significant improvement of the release patterns can be achieved by reversing the drug particle size distribution, i.e., drug particles of 1 μm are now located into the inner layer, and those of 10 μm into the outer one (Fig. 9b). Although the burst effect remains, release patterns are characterized by two regimes of nearly constant-rate release, displaying a definite break when the fine particles are entirely exhausted in the inner layer. This peculiar behavior is fully illustrated for the planar and cylindrical geometries. However, the first stage is only observable for the spherical geometry because the second one does not occur within the simulated times. From these results, two-layer matrix systems containing quite different particle sizes in each layer, with those of larger size into the outer one, appear to be suitable for approaching two successive drug release periods characterized by nearly constant release rates.

The effect of varying the relative thickness of the two layers can be easily studied by setting ξ^*, as desired. Instead of doing this type of analysis, we have preferred to simulate other more complex matrix architectures.

4.6. Example calculations for three-layer architectures

Composite matrices consisting of three-layers can be simulated using the following piecewise continuous distributions of drug:

$$C^0(\xi) = \Theta(\xi^* - \xi)C^0_{\text{inner}}(\xi) + \Theta(\xi - \xi^*)\Theta(\xi^{**} - \xi)C^0_{\text{middle}}(\xi) + \Theta(\xi - \xi^{**})C^0_{\text{outer}}(\xi) \quad (14a)$$

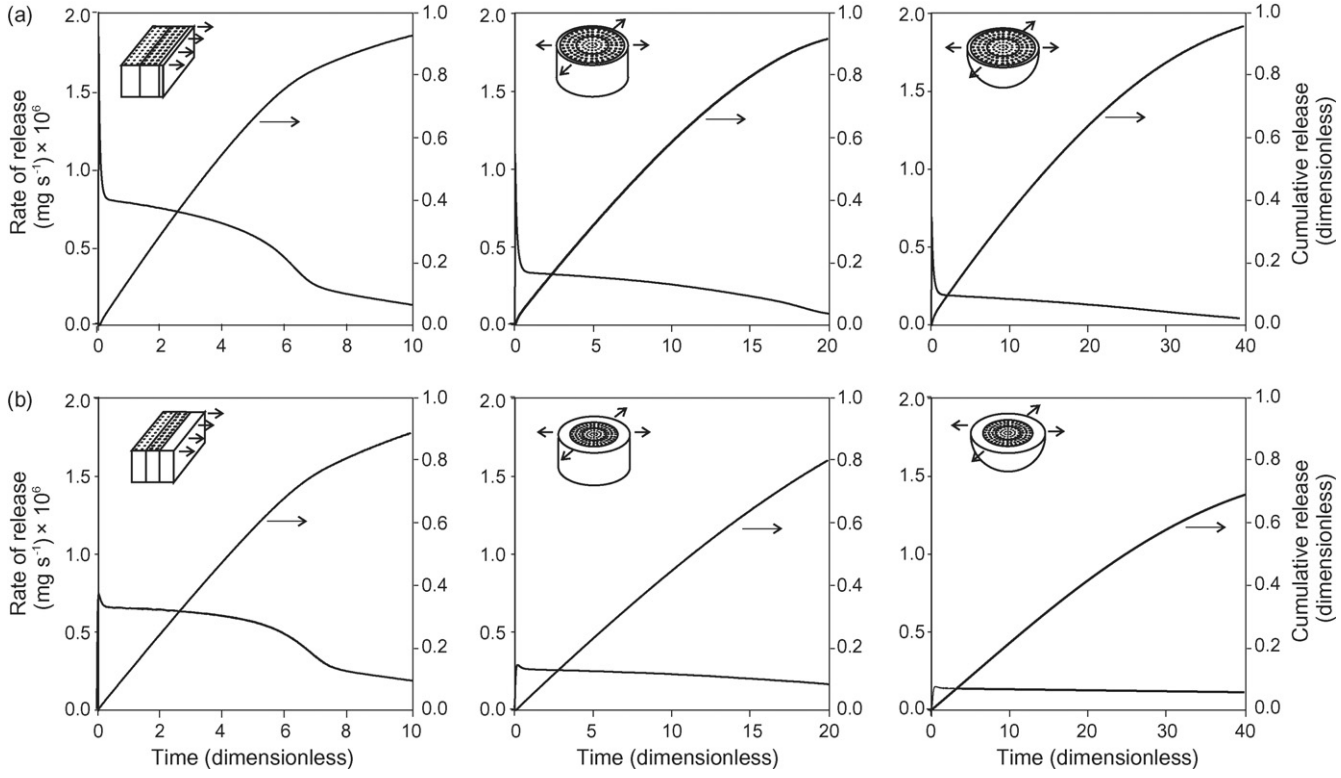

Fig. 10. Rate of drug release and cumulative release, as a function of time, for a total solid drug loading of 5% (w/v) spatially distributed in three-layers of different thickness. $C^0_{\text{inner}} = C^0_{\text{middle}} = 1$, $C^0_{\text{outer}} = 0$, $\varphi^0_{\text{inner}} = \varphi^0_{\text{middle}} = 0.025$, $\varphi^0_{\text{outer}} = 0$. (a) Relative thickness: $\xi^* = 0.45$ and $\xi^{**} = 0.90$; particle diameter from the center outwards: 1, 10 and 0 μm. (b) Relative thickness: $\xi^* = 0.33$ and $\xi^{**} = 0.66$; particle diameter from the center outwards: 1, 10 and 0 μm. The calculations were performed for $C_B = 0$; $L_c = 0.1$ cm; $D = 1 \times 10^{-8}$ cm^2 s^{-1}; $C_S = 5$ mg cm^{-3}; $\rho_S = 1.4$ g cm^{-3}; $Pe_B = 100$; $Pe_D = 0.1$.

$$\varphi^0(\xi) = \Theta(\xi^* - \xi)\varphi^0_{\text{inner}}(\xi) + \Theta(\xi - \xi^*)\Theta(\xi^{**} - \xi)\varphi^0_{\text{middle}}(\xi) + \Theta(\xi - \xi^{**})\varphi^0_{\text{outer}}(\xi) \quad (14b)$$

which reduce as follows:

$$C^0(\xi) = \begin{cases} C^0_{\text{inner}}(\xi) & 0 < \xi < \xi^* \\ C^0_{\text{middle}}(\xi) & \xi^* < \xi < \xi^{**} \\ C^0_{\text{outer}}(\xi) & \xi^{**} < \xi < 1 \end{cases} \quad (15a)$$

$$\varphi^0(\xi) = \begin{cases} \varphi^0_{\text{inner}}(\xi) & 0 < \xi < \xi^* \\ \varphi^0_{\text{middle}}(\xi) & \xi^* < \xi < \xi^{**} \\ \varphi^0_{\text{outer}}(\xi) & \xi^{**} < \xi < 1 \end{cases} \quad (15b)$$

where ξ^* is the dimensionless thickness of the inner layer, and $\xi^{**} - \xi^*$ is the dimensionless thickness of the middle layer. Example calculations are presented for inner and middle layers of identical thickness, and an empty outer layer, acting as membrane of equal diffusivity to that of the other two layers. For comparison purposes, the inner and middle layers are loaded with the same drug distribution as that used in the latter example of two-layer systems.

Fig. 10a and b displays how varying the thickness of the outer layer acting as membrane improves the release pattern. Results are illustrated for the case of drug particles of 1 μm located into the inner layer, and those of 10 μm into the outer one, as in Fig. 9b. The presence of the empty membrane diminishes or erases the burst effect, but the release pattern of further stages is not substantially modified with respect to those shown in Fig. 9b, for all three geometries. Indeed, a significant decrease of the burst effect is obtained by including a membrane of relative thickness 0.10 ($\xi^* = 0.45$ and $\xi^{**} = 0.90$), Fig. 10a, and a time-delayed release takes place for an increased relative thickness of 0.34 ($\xi^* = 0.33$ and $\xi^{**} = 0.66$), Fig. 10b.

The results so far presented demonstrate the effectiveness of this extended approach for the simulation of single-, two-, and three-layer matrix systems of planar, cylindrical, and spherical shapes containing arbitrary drug distributions. Analogous simulations can be done for any multi-layer architecture.

5. Conclusions

A generalized integral method (IM) for solving the design equations of dissolution/diffusion-controlled drug release from planar, cylindrical and spherical matrices has been provided, as an extension of a previously validated approach for planar matrices. The reliability of the approach was ascertained by comparing the results with existing analytical and numerical solutions for special cases, and also by matching, as asymptotic case, the numerical solution of the diffusion equation with a continuum dissolution source described by the Noyes–Whitney equation. The solution for the usual perfect sink condition was also obtained as special case. Some of the characteristics of the IM are as follows:

(1) The IM is suitable for handling spatially non-uniform drug distributions of both dissolved and undissolved drug, including piecewise continuous distributions, and arbitrary drug particle size distributions.
(2) The IM is effective for modeling dissolution and dissolution–diffusion drug release because the associated eigenvalue problems for all three geometries do not depend on the value of the Pe_D, so that once eigenvalues are calculated for a given Pe_B they become a result irrespective of whichever ratio between the dissolution and diffusion rates. While obvious, the usual solution for the perfect sink condition does not depend on the value of Pe_B.
(3) The IM is versatile for modeling symmetric multi-layer matrix systems of planar, cylindrical, and spherical geometries, within a unique framework and without introducing extra difficulties or adjustments in the programming from one matrix architecture to another. A unique dissolution–diffusion integral equation, coupled to the integral equations governing the variable surface area of the dissolving solid drug particles, must be solved using as well-established subroutines the corresponding eigenvalues and eigenfunctions data files to each geometry.
(4) The IM has proved suitable to devise a numerical solution based on iteration schemes combined with the homotopy method for the improvement of the numerical performance, especially for cylindrical and spherical geometries. The convergence of the iteration procedure can be achieved for a wide range of parameters having practical importance.
(5) The IM requires some training for solving numerically integral equations, the use of very refined homotopy paths would be excessively time consuming, and the treatment of multi-layer matrices is limited to layers of equal diffusivity.

Acknowledgements

The authors wish to express their gratitude to Agencia Nacional de Promoción Científica y Tecnológica (ANPCyT), to Consejo Nacional de Investigaciones Científicas y Técnicas (CONICET), and to Universidad Nacional del Litoral (UNL), Argentina, for the financial support granted to this contribution.

Appendix A. Derivation of Eq. (3b) as asymptotic case of Eq. (3a) as $N \to \infty$

Rearranging the third integral term of Eq. (3a) as follows:

$$Pe_D \int_0^\tau d\bar{\tau} \sum_1^N G(\xi, \tau; \xi_n, \bar{\tau})\sigma^0(\xi_n)\alpha(\xi_n, \bar{\tau})[1 - C(\xi_n, \bar{\tau})] = Pe_D \int_0^\tau d\bar{\tau} \sum_1^N \xi_n^p \Delta\xi_n G(\xi, \tau; \xi_n, \bar{\tau}) \frac{\sigma^0(\xi_n)}{\xi_n^p \Delta\xi_n} \alpha(\xi_n, \bar{\tau}) \times [1 - C(\xi_n, \bar{\tau})] \quad (A.1)$$

where $\Delta\xi_n$ is a subinterval of centre ξ_n and length $1/N$.

Taking the limit as $N \to \infty$, the R.H.S. of Eq. (A.1) becomes:

$$\lim_{N\to\infty} Pe_D \int_0^\tau d\bar{\tau} \sum_1^N \xi_n^p \, \Delta\xi_n G(\xi, \tau; \xi_n, \bar{\tau}) \frac{\sigma^0(\xi_n)}{\xi_n^p \, \Delta\xi_n} \alpha(\xi_n, \bar{\tau}) \times [1 - C(\xi_n, \bar{\tau})]$$
$$= Pe_D \int_0^\tau d\bar{\tau} \int_0^1 d\bar{\xi} \, \bar{\xi}^p G(\xi, \tau; \bar{\xi}, \bar{\tau}) \varphi^0(\bar{\xi}) \alpha(\bar{\xi}, \bar{\tau}) \times [1 - C(\bar{\xi}, \bar{\tau})] \quad (A.2)$$

where φ^0 is the initial surface area of solid drug particles per unit volume of matrix at position ξ, and α is the dimensionless surface area of the particles at position ξ and time τ.

Combining Eqs. (A.1) and (A.2), we obtain:

$$Pe_D \int_0^\tau d\bar{\tau} \sum_1^\infty G(\xi, \tau; \xi_n, \bar{\tau}) \sigma^0(\xi_n) \alpha(\xi_n, \bar{\tau}) [1 - C(\xi_n, \bar{\tau})]$$
$$= Pe_D \int_0^\tau d\bar{\tau} \int_0^1 d\bar{\xi} \, \bar{\xi}^p G(\xi, \tau; \bar{\xi}, \bar{\tau}) \varphi^0(\bar{\xi}) \alpha(\bar{\xi}, \bar{\tau}) \times [1 - C(\bar{\xi}, \bar{\tau})] \quad (A.3)$$

Substituting Eq. (A.3) into Eq. (3a), as $N \to \infty$, the resulting expression gives Eq. (3b), which is precisely the integral equation that would be obtained by applying the integral method to the diffusion equation with the Noyes–Whitney equation as continuum dissolution source in the $0 < \xi < 1$ interval.

Nomenclature

a	area of a solid drug particle at time t (cm^2 $particle^{-1}$)
A^e	external matrix cross-sectional area (cm^2)
C	dimensionless concentration ($=\hat{C}/C_S$)
$\hat{C}$	concentration of drug dissolved in the matrix ($g\,cm^{-3}$)
C_B	bulk concentration of drug ($g\,cm^{-3}$)
C_S	saturation concentration of the drug in the matrix ($g\,cm^{-3}$)
D	drug effective diffusivity ($cm^2\,s^{-1}$)
G	Green's function
k_B	external mass transfer coefficient ($cm\,s^{-1}$)
k_D	dissolution rate constant of the solid drug particle ($cm\,s^{-1}$)
L	half-thickness or radius of the matrix (cm)
L_c	characteristic length (cm) ($=VA^{-1} = L/(p+1)$)
N	number of solid drug particles dispersed into the matrix
N_n	number of solid drug particles at the drug dissolution source at ($\xi = \xi_n$)
p	geometric parameter defined in Eq. (1e)
Pe_B	Peclet number defined as the ratio between the diffusion and bulk mass transfer characteristic times ($=k_B L_c/D$)
Pe_D	Peclet number defined as the ratio between the diffusion and dissolution characteristic times ($=k_D L_c/D$)
Q	cumulative release
r_n	radius of the solid drug particles at ξ_n (μm)
s	auxiliary parameter into the homotopy method
t	time (s)
V	matrix volume (cm^3)
x	spatial coordinate (cm)

Greek symbols

α_n	dimensionless surface area of solid drug particle at ξ_n ($= a_n/a_n^0$)
β_m	mth eigenvalue defined in Tables 2 and 3
δ	Dirac delta function (cm^{-1})
δ_{nm}	Kronecker delta
Θ	Heaviside step function
$\varphi^0(\xi)$	initial overall surface area of the solid drug at ξ per volume unit matrix ($cm^2\,cm^{-3}$) ($=Na^0/V$)
ξ	dimensionless spatial coordinate ($=x/L_c$)
ρ_s	density of the solid drug ($g\,cm^{-3}$)
$\sigma^0(\xi_n)$	initial overall surface area of the solid drug at $\xi = \xi_n$ per external surface area unit matrix ($= \xi_n^p N_n a_n^0/A^e$)
τ	dimensionless time ($=tD/(L_c)^2$)
ϕ_m	mth eigenfunction defined in Tables 2 and 3
ψ_m	norm of the mth eigenfuntions defined in Tables 2 and 3

Superscripts

0	initial condition
* or **	interlayer boundary

References

[1] J. Siepmann, N.A. Peppas, Modeling of drug release from delivery systems based on hydroxypropyl methylcellulose (HPMC), Adv. Drug Deliv. Rev. 48 (2001) 139.

[2] T. Higuchi, Rate of release of medicaments from ointment bases containing drugs in suspension, J. Pharm. Sci. 50 (1961) 874.

[3] D.R. Paul, S.K. McSpadden, Diffusional release of a solute from a polymeric matrix, J. Membr. Sci. 1 (1976) 33.

[4] P.I. Lee, Diffusional release of a solute from a polymeric matrix-approximate analytical solutions, J. Membr. Sci. 7 (1980) 256.

[5] M.J. Abdekhodaie, Y.-I. Cheng, Diffusional release of a dispersed solute from a spherical polymer matrix, J. Membr. Sci. 115 (1996) 171.

[6] A.L. Bunge, Release rates from topical formulations containing drugs in suspension, J. Control. Release 52 (1998) 141.

[7] T. Higuchi, Mechanism of sustained action medication: theoretical analysis of rate of release of solid drugs dispersed in solid matrices, J. Pharm. Sci. 52 (12) (1963) 1145.

[8] T.J. Roseman, W.I. Higuchi, Release of medroxyprogesterone acetate from a silicone polymer, J. Pharm. Sci. (1970) 353.

[9] R.A. Lipper, W.I. Higuchi, Analysis of theoretical behaviour of a proposed zero-order drug delivery system, J. Pharm. Sci. 66 (1977) 163.

[10] W.D. Rhine, D.S.T. Hsieh, R. Langer, Polymers for sustained macromolecule release: procedures to a fabricate reproducible delivery systems and control release kinetics, J. Pharm. Sci. 69 (1980) 265.

[11] S. Béchard, J.N. Mc Mullen, Solute release form a porous polymeric matrix: inwardly tapered disk with a central releasing hole, J. Pharm. Sci. 77 (1988) 222.
[12] D.S.T. Hsieh, W.D. Rhine, R. Langer, Zero-order controlled release polymer matrices for micro- and macro-molecules, J. Pharm. Sci. 72 (1983) 17.
[13] B. Narasimhan, R. Langer, Zero-order release of micro- and macromolecules from polymeric devices: the role of the burst effect, J. Control. Release 47 (1997) 13.
[14] R.A. Siegel, Theoretical analysis of inward hemispheric release above and below drug solubility, J. Control. Release 69 (2000) 109.
[15] P.I. Lee, Effect of non-uniform initial drug concentration distribution on the kinetics of drug release from glassy hydrogel matrices, Polymer 25 (7) (1984) 973.
[16] S. Lu, W.F. Ramirez, K.S. Anseth, Modeling and optimization of drug release from laminated polymer matrix devices, AIChE J. 44 (7) (1998) 1689.
[17] Y. Zhou, X.Y. Wu, Finite element analysis of diffusional drug release from complex matrix systems. I. Complex geometries and composite structures, J. Control. Release 49 (1997) 277.
[18] Y. Zhou, X.Y. Wu, Finite element analysis of diffusional drug release from complex matrix systems. II. Factors influencing release kinetics, J. Control. Release 51 (1998) 57.
[19] Y.W. Chien, H.J. Lambert, D.E. Grant, Controlling drug release from polymeric devices. I. Technique for rapid in vitro release studies, J. Pharm. Sci. 63 (1974) 365.
[20] K. Tojo, Intrinsic release rate from matrix-type drug delivery systems, J. Pharm. Sci. 74 (1985) 685.
[21] M.J. Abdekhodaie, Y.-I. Cheng, Diffusional release of a dispersed solute from planar and spherical matrices into finite external volume, J. Control. Release 43 (1997) 175.
[22] X.Y. Wu, Y. Zhou, Studies of diffusional release of a dispersed solute from polymeric matrixes by finite element method, J. Pharm. Sci. 88 (10) (1999) 1050.
[23] Y. Zhou, X.Y. Wu, Theoretical analyses of a dispersed-drug release from planar matrices with a boundary layer in a finite medium, J. Control. Release 84 (2002) 1.
[24] D.R. Paul, Modeling of solute release from laminated matrices, J. Membr. Sci. 23 (1985) 221.
[25] G.Ch. Charalambopoulou, E.S. Kikkinides, K.G. Papadokostaki, A.K. Stubos, A.Th. Papaioannou, Numerical and experimental investigation of the diffusional release of a dispersed solute from polymeric multilaminate matrices, J. Control. Release 70 (2001) 309.
[26] J.W. Ayres, F.T. Lindstrom, Diffusion model for drug release from suspensions. I. Release to a perfect sink, J. Pharm. Sci. 66 (1977) 662.
[27] S.K. Chandrasekaran, D.R. Paul, Dissolution-controlled transport from dispersed matrices, J. Pharm. Sci. 71 (1982) 1399.
[28] R.S. Harland, C. Dubernet, J.-P. Benoit, N.A. Peppas, A model of dissolution-controlled diffusional drug release from non-swellable polymeric microspheres, J. Control. Release 7 (3) (1988) 207.
[29] N.J. Chang, K.J. Himmesltein, Dissolution–diffusion controlled constant rate release from heterogeneously loaded drug-containing materials, J. Control. Release 12 (1990) 201.
[30] R.T. Kurnik, R.O. Potts, Modeling of diffusion and crystal dissolution in controlled release systems, J. Control. Release 45 (1997) 257.
[31] G. Frenning, Theoretical investigation of drug release from planar matrix systems: effects of a finite dissolution rate, J. Control. Release 92 (2003) 331.
[32] G. Frenning, Theoretical analysis of the release of slowly dissolving drugs from spherical matrix systems, J. Control. Release 95 (2004) 109.
[33] A.A. Noyes, W.R. Whitney, The rate of solution of solid substances in their own solutions, J. Am. Chem. Soc. 19 (1897) 930.
[34] M.I. Cabrera, J.A. Luna, R.J.A. Grau, Modeling of dissolution–diffusion controlled drug release from planar polymeric systems with finite dissolution rate and arbitrary drug loading, J. Membr. Sci. 280 (2006) 693.
[35] M.N. Ozişik, Heat Conduction, John Wiley and Sons, New York, 1993.
[36] E.A. Coddington, N. Levinson, Theory of Ordinary Differential Equations, Mc-Graw-Hill, New York, 1955.
[37] B. Tabis, Criterion for the uniqueness of steady states in non-adiabatic tubular reactors, Int. Chem. Eng. 26 (1986) 746.
[38] B. Tabis, An iterative computation method of chemically reacting systems with distributed state variables, in: N. Cheremisinoff (Ed.), Handbook of Heat and Mass Transfer, vol. 3, Gulf, Houston, 1989, p. 1173.
[39] H. Cantero, R.J.A. Grau, M.A. Baltanás, Cocurrent turbulent tubereactor with multiple gas injections and recycle of slurry: a treatment in terms of Green functions, Comput. Chem. Eng. 18 (7) (1994) 551.
[40] M.I. Cabrera, R.J.A. Grau, A.E. Cassano, The laminar flow tubular reactor with homogeneous and heterogeneous reactions. II. Application to reactor modeling involving free radical reactions, Chem. Eng. Commun. 185 (2001) 23.
[41] D.E. Müller, A method for solving algebraic equations using an automatic computer, Math. Tables Aids Comput. 10 (1956) 208.
[42] R.P. Brent, An algorithm with guaranteed convergence for finding a zero of a function, Comput. J. 14 (1971) 422.
[43] F.B. Hildebrand, Introduction to Numerical Analysis, McGraw Hill, New York, 1956.
[44] J. Crank, The Mathematics of Diffusion, Oxford University Press, London, 1975.